Reac Kinet Mech Cat (2017) 120:459–475
DOI 10.1007/s11144-016-1110-x

Dry reforming of methane on grafted-supported Rh catalysts: effect of the metal-support interaction on the reaction rate

Yayné Beltrán[1] · Camila Fernández[2] · Gina Pecchi[1] · Romel Jiménez[2]

Received: 25 July 2016 / Accepted: 9 November 2016 / Published online: 17 November 2016

Abstract Catalysts of rhodium supported on pure oxides and modified alumina with 50, 75 and 100% of ZrO_2 were prepared by the impregnation method, to be tested in the reaction of dry reforming of methane in order to study the effect of the metal-support interaction on the reaction rate. The catalysts were characterized by N_2 adsorption isotherms, CO chemisorption, TEM, temperature programmed reduction, XRD and XPS. The reaction rate for CH_4 conversion was measured at 500–700 °C, in the absence of transport limitation. The average Rh cluster size in catalysts with modified supports resulted similar as compared with the catalyst Rh/0%ZrO_2–Al_2O_3, so that the modification of the support had no effect on the dispersion of Rh, which is associated with the similarity in the BET surface area of the pure and modified alumina. The Rh-support interaction is determined by the degree of coverage of alumina with zirconia and by the nature of ZrO_2 phase formed in the grafted supports. The higher coverage of alumina with zirconia leads to a lower Rh-support interaction. However, the interaction of Rh with the monoclinic phase seems to be weaker than with the tetragonal phase of zirconia, the latter more abundant as the loading of ZrO_2 is increased in the grafted supports. Consequently, the Rh-support interaction increases with the content of ZrO_2. Despite the different Rh-support interaction, the structural sensitivity of dry reforming of methane on Rh catalysts was still evidenced, i.e., the DRM reaction rate is mainly determined by the coordination degree of Rh atoms on the catalyst surface.

✉ Romel Jiménez
romeljimenez@udec.cl

[1] Department of Physical Chemistry, Faculty of Chemical Sciences, University of Concepción, Concepción, Chile

[2] Department of Chemical Engineering, Faculty of Engineering, University of Concepción, Concepción, Chile

Keywords Rhodium · Dry reforming of methane · Metal-support interaction · Grafting

Notation

X	Conversion
a, b, c, d	Stoichiometric coefficient
A, B, C, D	Reaction component
w	Catalyst weight (g)
F_{A0}	Initial A reactant flow (mol s^{-1})
r_A	Observed (net) reaction rate (mol g_{cat}^{-1} s^{-1})
r_f	Forward reaction rate (mol g_{cat}^{-1} s^{-1})
η	Approach to equilibrium
k	Constant rate (mol g_{cat}^{-1} s^{-1} kPa^{-1})
P_i	Partial pressure of species (kPa)
K_{eq}	Equilibrium constant
R	Universal gas constant (8.3145 J mol^{-1} K^{-1})

Introduction

The negative effects of the primary greenhouse gases CO_2 and CH_4 on the environment have been widely evidenced [1, 2]. However, the mitigation of these pollutants is still a crucial challenge for governments, industrialists and scientists. Fortunately, carbon dioxide is being increasingly considered as a valuable feedstock for the chemical industry and fuel companies rather than a waste with a high cost of disposal, in addition to the many benefits that it means in terms of positive image for the companies [2, 3].

Among the different options to covert CO_2 into valuable products (methane, methanol, hydrocarbons, syngas), the dry reforming of methane (DRM) to produce CO and H_2 represents a scientifically interesting and technically attractive alternative, especially for the use of natural gas deposits, where CO_2 and CH_4 are present together. The DRM process is thus useful to simultaneously consume both greenhouse gases and produce *syngas*, which is considered a commodity since it is a feedstock for the production of higher hydrocarbons by the Fischer–Tropsch synthesis (FT) and for carbonylation processes [1, 4–7]. In addition, DRM represents an advantageous route for the storage of renewable energy source due to its high reaction enthalpy [5].

Al_3O_2-supported Ni catalysts have shown high activity for DRM, but the major drawback observed is the high carbon formation, resulting in a fast catalyst deactivation [1, 6]. In fact, it is considered that the catalyst reactivity and stability for the dry reforming of CH_4 strongly depend on the catalyst's resistance to carbon deposits, which could lead to the blockade of active sites [8]. The replacement of Ni by noble metals has shown to lead to very high activity and lower catalyst

deactivation, despite their higher cost. Even though Rh is considered one of the most effective noble metals for DRM [1, 2, 4, 5, 8, 9], the interaction between Rh particles and the support may affect the catalytic activity and stability for long term reaction conditions [10, 11]. Specifically, Al_2O_3-supported Rh catalysts have shown high activity for DRM since alumina provides a large and mechanically stable surface area where Rh particles can properly disperse [1, 5, 11]. However, the high temperatures needed for DRM reaction (500–700 °C) lead to severe catalyst deactivation, due to the strong interaction between rhodium oxide and alumina, which drastically decreases the reducibility of rhodium atoms at the surface [8, 9].

To avoid this problem, grafting of ZrO_2 over alumina prior to the impregnation of Rh precursor has been used with dual purpose: (i) ZrO_2 acts as a barrier to decrease the Rh-alumina interaction [9] by avoiding the formation of metal aluminate (rhodium aluminate) [4], and (ii) ZrO_2 can play an important role in the oxidation of carbon deposit since it is considered a so-called oxy-transporter support, thus allowing a higher stability of the catalysts [4, 12]. Additionally, because of its redox properties, this kind of support is reported to actively participate in the catalytic reaction by oxidizing or reducing reaction intermediates [2]. The grafting method is very advantageous, since it leads to a great number of high quality contacts between the support and the metal oxides incorporated on its surface, with high dispersion, high resistance to sintering and good mechanical properties [7, 13].

It has been shown that the kinetically relevant step for DRM is the C-H bond activation on the catalyst surface. This is a structure sensitive reaction favored in stepped and kinked surfaces with prevalence of low-coordinated atoms, which are proportionally more abundant in small particle clusters [14–16]. It has also been reported that the support nature has practically no effect on the CH_4 reforming rate on Rh particles, as similar cluster sizes on different supports have shown similar activities; however, the effect of Rh-support interaction on the specific Rh activity has not been directly evaluated.

In this work, we use the grafting technique to incorporate ZrO_2 over Al_2O_3 in order to modify the interaction between support and Rh, incorporated by impregnation of rhodium precursor on the grafted supports. The change in the Rh-support interaction as Al_2O_3 is modified with ZrO_2 is experimentally evidenced, and the CH_4 reforming rate on Rh catalysts with different extent of metal-support interaction is measured and compared in terms of forward CH_4 conversion rate. The reaction rates are measured in a differential reactor and finally corrected by the approach to equilibrium factor; for CH_4 conversion higher than 10% (integral reactor) the forward reaction rate is calculated from integration by considering a first-order kinetics on CH_4 pressure [15]. The effect of Rh-support interaction on the well-reported structure sensitivity of DRM reaction is properly evaluated and discussed.

Experimental

Catalysts preparation

Supports

The alumina modified with zirconia was prepared by the method of grafting coating. The grafting procedure was carried out by adding the γ-Al_2O_3 support (Alfa Aesar, SBET = 72 m^2 g^{-1}) to a solution of zirconium(IV) *n*-propoxide (Merck, 99.8%) in *n*-propanol (Merck 99.8%). The amount of Zr precursor required to form a ZrO_2 theoretical monolayer on the alumina surface, was calculated by considering a conventional stoichiometry of one ZrO_2 molecule to one hydroxyl group, and that the ZrO_2 molecule has a circular projection with a radius equal to 0.226 nm [7]; this amount corresponds to 9.6 wt% of ZrO_2 in the γ-Al_2O_3 support). After stirring for 2 h at room temperature and connected to a vacuum rotary evaporator at 30 °C under reduced pressure for slowly removing the solvent, the material was dried in an oven for 16 h at 110 °C. The ZrO_2 coating percent were: 50, 75 and 100%. The pure and modified supports were calcined at 500 °C in air for 5 h with a heating rate of 10 °C min^{-1}.

Rh catalysts

The metal phase, 1% Rh, was incorporated into the supports by wet impregnation of ammonium hexachloroiridate (Alfa Asear, 28 wt% of Rh). The precursor dissolution in deionized water added to the previously prepared support and stirred for 2 h at room temperature, the solvent was evaporated in rotavapor at 35 °C under reduced pressure followed by drying in an over at 110 °C and calcined in air at 700 °C for 4 h at a heating rate of 10 °C min^{-1}.

Catalysts characterization

The specific area was measured by N_2 (Indura S.A, >99.9%) adsorption isotherms at 77 K (temperature of liquid N_2) on a Micromeritics Gemini 2360 instrument. The sample is previously out-gassed under vacuum at 300 °C for 24 h. The specific area was calculated according to the BET method and the total pore volume (V_P) was taken at a relative pressure of 0.99.

Rh dispersion was measured by irreversible CO (Indura S.A., >99.9%) pulse chemisorption in a Chem BET Pulsar TPR/TPD (Quatachrome Instruments). Then the catalyst is reduced in pure hydrogen (30 mL min^{-1}) by heating up to 700 at 10 °C min^{-1}. Reached 700 °C, this temperature is maintained for 2 h. It is assumed a stoichiometry of adsorption CO/Rh = 1 (CO adsorbed to surface Rh-atoms ratio).

TEM micrographs were obtained in a Jeol JEM-1200 EX II microscope. The samples were prepared by the carbon replica technique, in an evaporating unit, evacuated and carbon evaporated onto the solid by passing a high current between two carbon rods. After a thick film of carbon coats on the sample, it is placed in a

60HF/40$HClO_4$ dissolution enough time to remove the mixed oxides by a chemical attack. Consequently, the observed particles correspond to Rh nanoparticles, and the differences in contrast are attributed to electrons scattered outside the objective aperture.

Programmed reduction temperature (H_2-TPR) assays were carrying out in a ChemBET Pulsar TPR/TPD equipped with a TCD. The change in the gas thermal conductivity was registered as a function of temperature. Typically, 150 mg of sample was heated at 10 °C min^{-1} from ambient temperature up to 700 °C, in 30 mL min^{-1} of 5% H_2/Ar gas mixture (Indura S.A., >99.9%). After reaching 700 °C, the reducing conditions were maintained for 2 h. The amount of H_2 consumed is quantified by using a calibration curve, previously obtained from a calibration test with CuO in the same operating conditions.

X-ray photoelectron spectra were obtained for calcined and tested samples with a SSI-X-probe (SSX-100/206) spectrometer equipped with a monochromatized microfocused Al K_α X-ray source, operating at 10 kV and 12 mA. After outgassing under vacuum (10^{-5} Torr) overnight, the samples were placed in the analysis chamber where the residual pressure was of about 10^{-7} Torr. The charging effect was adjusted using flood gun energy at 8 eV and a fine-meshed nickel grid, placed 3 mm above the sample surface. The pass energy was 150 eV, and the spot size was 1000 μm. The angle between the normal to the sample surface and the direction of electron collection was 55°. The binding energy scale of the spectrometer was calibrated with respect to the Au $4f_{7/2}$ peak of gold, fixed at 83.98 eV, and the binding energies of O 1s, Al 2p, Zr 3d, and Rh 3d were referenced to the C–(C,H) component of C 1s band, fixed at 284.8 eV.

In order to obtain surface atomic concentrations, relative areas of corresponding peaks were normalized by sensitivity factors based on Scofield cross-sections. Peak decomposition was performed using the CasaXPS program (Casa Software, UK), assuming an 85/15 Gaussian/Lorentzian product function and a Shirley non-linear sigmoid-type baseline. The 'percentage of monolayer dispersion' of supports was estimated according to the model proposed by Kerkhof et al. [17], which considers cubic particles 'p' deposited over support sheets 's'. The thickness (t) of these sheets is obtained from the support density (ρ_s) and surface area ($S_{BET,s}$), as shown below:

$$t = \frac{2}{\rho_s S_{BET,s}}. \tag{1}$$

According to this model, the theoretical XPS $(p/s)_m$ atomic ratio expected for a monolayer dispersion of particles on the support is given by:

$$\left(\frac{p}{s}\right)_m = \left(\frac{p}{s}\right)_{bulk} \frac{G(\varepsilon_p)}{G(\varepsilon_s)} \frac{\sigma_p}{\sigma_s} \frac{1}{2} \left(\frac{t}{\lambda_{s-s}}\right) \frac{1+\exp(-t/\lambda_{p-s})}{1-\exp(-t/\lambda_{p-s})}, \tag{2}$$

Here G functions of the electron kinetic energies (ε) correspond to the spectrometer efficiencies and can be approximated as ε^{-1} [18]. σ_p and σ_s are the relative photoelectron cross sections provided by Scofield [19]. λ_p and λ_s correspond to the escape depths of photoelectrons from the particles and support through the support,

and can be determined by the Tanuma et al. [18] algorithm, using the QUASES-IMFP-TPP2M software [20].

$(p/s)_{bulk}$ is the nominal bulk atomic ratio, calculated from the nominal mass (m_j) and atomic or molecular mass (M_j) of the particles and support materials, as follows:

$$(p/s)_{bulk} = \frac{m_p M_s}{2 m_s M_p}. \quad (3)$$

The 'percentage of monolayer dispersion' of particles 'p' on the support 's' is then expressed as the experimental ratio relative to the calculated one, as follows:

$$\% \text{ of monolayer dispersion} = \frac{(p/s)_{exp}}{(p/s)_m} \cdot 100. \quad (4)$$

It is noteworthy that this is not a direct measurement of dispersion, defined as the fraction of 'p' atoms exposed at surface, from the total amount of 'p' atoms present in the catalyst, which is inversely proportional to the particle size. According to the Kerkhof model (assuming cubic supported particles), the 'percentage of monolayer dispersion' as a function of the particle size (d) is expressed as follows:

$$\frac{(p/s)_{exp}}{(p/s)_m} = \frac{1 - \exp(-d/\lambda_{p-p})}{d/\lambda_{p-p}}. \quad (5)$$

Catalytic activity

The steady-state CH_4 conversion rates were measured in a tubular packed-bed quartz reactor (8 mm inner diameter) with plug-flow hydrodynamics under differential ($X_{CH4} < 15\%$) or integral ($X_{CH4} > 15\%$) conditions. 50 mg of the catalyst (dp 104–180 μm) are supported on a quartz frit and two K-type thermocouples located in the center of the furnace and inside the reactor near the bed control and measure the reaction temperature, respectively. In all experiments, both temperatures were similar. Previous tests define the reaction conditions to ensure the absence of heat and mass transport limitations [7, 21].

Before performing the reaction, the catalyst is reduced in situ in pure H_2 (Air Liquide S.A., 99.99%) flow (80 mL min^{-1}) increasing the temperature since room temperature to 700 °C for 2 h. Then, the system is purged in He (Air Liquide S.A., 99.999%) for 30 min.

Next, the reactor is cooled down in He to 500 °C to start the isothermal catalytic tests, the temperature is increased 50 °C from 500 to 700 °C, and finally the starting point is repeated at 500 °C in order to evaluate catalyst deactivation. The reaction is carried out in a flowing mixture (100 mL min^{-1}) of CH_4/CO_2/He (10/20/70 vol%) and a space velocity of 1.2×10^5 mL h^{-1} g_{cat}^{-1}. A high dilution in helium allows to manage the rate of heat production, avoiding cold spots that could promote undesirable reactions such as the reverse Boudouard reaction ($2CO \rightarrow C + CO_2$) [7].

The concentrations of CH_4, CO, CO_2 and H_2 in the inlet and outlet streams are measured by using a GC PERKIN ELMER 8700 GC equipped with a thermal conductivity detector (TCD), a flame ionization detector (FID) and a Carboxen adsorption column 80/60 (Supelco). For reactor operation under differential conditions, the measured CH_4 conversion rate is directly calculated from Eq. 6. For the integral reactor performance ($X_{CH4} > 10\%$), the reaction rate constant is calculated from Eq. 25 (numerically solved using MATLAB 8.0000) by considering a first order dependence on the CH_4 pressure as previously reported [15], then the reaction rate was calculated by Eq. (11) and the forward CH_4 conversion rates are calculated using the approach to equilibrium parameter [Eq. 23] and normalized by exposed Rh atoms.

$$r_{CH_4} = \frac{X}{(W \cdot F_{CH_4 0})}; \tag{6}$$

Mathematical treatment of the integral reactor

The dry reforming reaction of methane, Eq. 7a and the general expression by Eq. 7b:

$$CH_4(g) + CO_2(g) \leftrightarrow 2CO(g) + 2H_2(g); \tag{7a}$$

$$aA(g) + CO_2(g) \leftrightarrow 2CO(g) + 2H_2(g); \tag{7b}$$

Considering the equation for a packed bed reactor, Eq. 8 and the reaction rate [15, 22], Eq. 9:

$$W = F_{A_0} \int_0^x \frac{dx}{-r_A}; \tag{8}$$

$$-r_A = r_f(1 - \eta); \tag{9}$$

Substituting Eq. 9 into Eq. 8:

$$W = F_{A_0} \int_0^x \frac{dx}{r_f(1 - \eta)}; \tag{10}$$

Is has been reported for dry reforming of methane, the reaction rate depends only on the partial pressure of methane [14, 15], Eq. 11.

$$r_f = k \cdot P_{CH_4}; \tag{11}$$

And the approach to equilibrium (η) is a relationship between the pressures of the products, reactants and the equilibrium constant [15], by Eq. 12.

$$\eta = \frac{P_{CO}^2 \cdot P_{H_2}^2}{P_{CO}^2 \cdot P_{CH_4}^2} \cdot \frac{1}{K_{eq}}; \tag{12}$$

The concentrations in a gas flow system of constant volume can be calculated by the following expressions [23]:

$$C_A = C_{A_0} \frac{1 - X}{1 + \varepsilon \cdot X} \cdot \left(\frac{T_0}{T}\right) \cdot \left(\frac{P}{P_0}\right); \tag{13}$$

$$C_B = C_{A_0} \frac{\theta_B - (b/a)X}{1 + \varepsilon \cdot X} \cdot \left(\frac{T_0}{T}\right) \cdot \left(\frac{P}{P_0}\right); \tag{14}$$

$$C_C = C_{A_0} \frac{\theta_C - (c/a)X}{1 + \varepsilon \cdot X} \cdot \left(\frac{T_0}{T}\right) \cdot \left(\frac{P}{P_0}\right); \tag{15}$$

$$C_D = C_{A_0} \frac{\theta_d - (d/a)X}{1 + \varepsilon \cdot X} \cdot \left(\frac{T_0}{T}\right) \cdot \left(\frac{P}{P_0}\right); \tag{16}$$

Considering the stoichiometry for the reaction of dry reforming of methane, there is a change in volumetric flow as a result of the change in the number of total moles that exit with respect to the total moles of reactants. Therefore, $\delta = \frac{d}{a} + \frac{c}{a} + \frac{b}{a} + 1 = 2$, $\varepsilon = \delta \cdot y_{CH_{4,0}}$, and $\varepsilon = 0.2$ for the experimental system, by using the initial concentration of the limiting reactant A.

Considering an isobaric and isothermal system: $\left(\frac{T_0}{T}\right) = 1$, $\left(\frac{P}{P_0}\right) = 1$.

Also $\theta_i = \frac{C_{i,0}}{C_{A,0}} = \frac{y_{i,0}}{y_{A,0}} = \frac{P_{i,0}}{P_{A,0}}$, then $\theta_B = 2$, $\theta_C = \theta_D = 0$.

Substituting in Eqs. 13–16 is obtained:

$$C_A = C_{A_0} \frac{1 - X}{1 + \varepsilon \cdot X}; \tag{17}$$

$$C_B = C_{A_0} \frac{\theta_B - (b/a)X}{1 + \varepsilon \cdot X}; \tag{18}$$

$$C_C = C_{A_0} \frac{\theta_C - (c/a)X}{1 + \varepsilon \cdot X}; \tag{19}$$

The ideal gas law ($C_C = \frac{P_i}{R \cdot T}$) is used to express concentrations of Eqs. 17–19 in terms of the partial pressure of methane for all reaction components, leading to Eqs. 20–22:

$$P_{CH_4} = P_{CH_{4,0}} \cdot \frac{1 - X}{1 + \varepsilon \cdot X}; \tag{20}$$

$$P_{CO_2} = P_{CH_{4,0}} \cdot \frac{2 - X}{1 + \varepsilon \cdot X}; \tag{21}$$

$$P_{CO} = P_{H_2} = P_{CH_{4,0}} \cdot \frac{2X}{1 + \varepsilon \cdot X}; \tag{22}$$

Substituting Eqs. 20–22 into Eqs. 12 and 11 gives:

$$\eta = \frac{\left(P_{CH_{4,0}} \cdot \frac{2X}{1+\varepsilon \cdot X}\right)^2 \cdot \left(P_{CH_{4,0}} \cdot \frac{2X}{1+\varepsilon \cdot X}\right)^2}{\left(P_{CH_{4,0}} \cdot \frac{2-X}{1+\varepsilon \cdot X}\right) \cdot \left(P_{CH_{4,0}} \cdot \frac{1-X}{1+\varepsilon \cdot X}\right)} \cdot \frac{1}{K_{eq}}$$

$$\eta = 16 \cdot \frac{P_{CH_{4,0}}^2}{K_{eq}} \cdot \frac{X^4}{(1 - X)(2 - X)\,(1 + \varepsilon \cdot X)^2}; \tag{23}$$

$$r_f = k \cdot P_{CH_{4,0}} \cdot \frac{1 - X}{1 + \varepsilon \cdot X}; \tag{24}$$

Substituting Eqs. 23 and 15 into Eq. 9 leads to Eq. 25:

$$k = \frac{F_{A_0}}{W \cdot P_{CH_{4,0}}} \int_0^X \left(\frac{1 - X}{1 + \varepsilon \cdot X} - 16 \cdot \frac{P_{CH_{4,0}}^2}{K_{eq}} \cdot \frac{X^4}{(2 - X)\,(1 + \varepsilon \cdot X)^3} \right)^{-1} dx \tag{25}$$

The equilibrium constant at reaction condition, K_{eq} (T), is determined from van't Hoft equation [Eq. 27], while the equilibrium constant at standard condition (1 atm, 298.15 K) is calculated from Eq. 26. Working with the van't Hoft equation and assuming that the change in the enthalpy of reaction ($\Delta H°_r$) is independent of temperature, the equilibrium constant at a given temperature is determined from Eq. 27. The value of $\Delta H°_r$ is determined from the normal enthalpies of formation at standard conditions [24, 25] and taking into account the stoichiometry of DRM reaction [Eq. 7a].

$$\Delta G^0 = -R \cdot T \cdot \ln\left(K_{EQ}^0\right); \tag{26}$$

$$K_{eq}(T) = K_{EQ}^0 \cdot \mathrm{Exp}\left[\frac{\Delta H^0}{R}\left(\frac{1}{T^0} - \frac{1}{T}\right)\right]; \tag{27}$$

Results and discussion

Catalytic activity

Table 1 shows the conversion of methane during DRM performed on supported Rh catalysts, at 500–700 °C and steady state reaction conditions. The two non-modified-supported Rh catalysts (Rh/ZrO_2 and $Rh/0\%ZrO_2–Al_2O_3$) lead to

Table 1 Catalytic activity of supported Rh catalysts for the DRM at 500–700 °C, 10 kPa CH_4/20 kPa CO_2/He balance; 1.2×10^5 mL h^{-1} g_{cat}^{-1}

Catalyst	% CH_4 conversion						E_{ap}
	500 °C	550 °C	600 °C	650 °C	700 °C	500 °C	kJ mol^{-1}
Rh/0%ZrO_2–Al_2O_3	17	31	51	74	92	17	89.3
Rh/50%ZrO_2–Al_2O_3	19	35	55	75	91	20	82.7
Rh/75%ZrO_2–Al_2O_3	17	32	50	67	85	19	75.0
Rh/100%ZrO_2–Al_2O_3	20	34	56	78	94	20	88.6
Rh/ZrO_2	3	4	7	14	24	2	89.1

significantly different CH_4 conversions: CH_4 conversion on Rh/0%ZrO_2–Al_2O_3 is about one order of magnitude higher than on Rh/ZrO_2, both measured under similar reaction conditions and equal mass of catalyst in the fixed bed reactor (50 mg). Similar methane conversions are observed for the non-modified Rh/0%ZrO_2–Al_2O_3 and the ZrO_2–Al_2O_3-supported Rh catalysts. Rh/100%Zr–Al_2O_3 catalyst shows the highest activity among grafted-support catalysts.

The conversion at the initial reaction condition (500 °C) was double-checked at the end of each set of catalytic tests (about 9 h in continuous operation, from 500 to 700 °C) in order to evaluate the deactivation of the catalysts; results of this final measurement are also included in Table 1. No significant differences are observed between the initial and final measurements, and the deactivation of catalysts can be therefore excluded. Additionally, reproducibility was confirmed by repeating the catalytic tests at a given reaction condition, after flushing the catalytic bed with He overnight, at room temperature (not shown). The excellent reproducibility for CH_4 conversion (differences below 2%) was confirmed for all measurements.

Textural and structural properties of catalysts

The addition of zirconia to Al_2O_3 via the grafting procedure does not significantly affect the specific surface area of the support (Table 2), which suggests that the ZrO_2 ($S_{BET} = 4$ m^2 g^{-1}) is properly dispersed over alumina surface and it does not block the pores of the support structure. Moreover, the thermal treatment used in the synthesis of grafted supports (500 °C in air for 5 h) seems not to cause sintering of the support. However, the grafting procedure provokes a change in the nature of ZrO_2 phases (Fig. 1). In fact, the formation of tetragonal ZrO_2 phases (peaks at $2\theta \approx 30.2°$, 50.2° and 60°) increases with the content of zirconia in the grafted support while the monoclinic phase ($2\theta \approx 24°$, 28.2°, 31.5° and 41°) predominates in the commercial ZrO_2 oxide used as pure support in Rh/ZrO_2 catalyst.

The S_{BET} values decrease in more than 15% after impregnation of the active phase (1% Rh) on both non-modified and grafted supports and subsequent calcination at 700 °C for 4 h. This is mainly attributed to the sintering process that occurs due to calcination at high temperatures (700 °C). Additionally, the higher peaks associated to the tetragonal ZrO_2 phases observed for the catalysts (Fig. 1b)

Table 2 Textural properties for supports and supported Rh catalysts: Rh dispersion estimated by CO chemisorption [D_{Rh} (ch)]; % of monolayer dispersion for Rh on catalyst [D_{Rh} (XPS)] and for ZrO_2 on grafted supports [D_{ZrO_2} (XPS)], calculated from XPS data; mean cluster size estimated from CO chemisorption (d_{ch}) and measured by TEM (d_{TEM})

	S_{BET} (m^2 g^{-1})	Pore volume (cm^3 g^{-1})	D_{Rh} (ch)	D_{Rh} (XPS)	D_{ZrO2} (XPS)	d_{ch} (nm)	d_{TEM} (nm)
0%ZrO_2–Al_2O_3	73	0.25	–	–	–	–	–
50%ZrO_2–Al_2O_3	75	0.17	–	–	14.5	–	–
75%ZrO_2–Al_2O_3	76	0.18	–	–	29.1	–	–
100%ZrO_2–Al_2O_3	78	0.18	–	–	12.3	–	–
Rh/0%ZrO_2–Al_2O_3	60	0.23	0.31	0.41	–	3.5	3.1
Rh/50%ZrO_2–Al_2O_3	58	0.19	0.25	0.52	20.3	4.5	–
Rh/75%ZrO_2–Al_2O_3	57	0.19	0.28	0.62	26.7	3.9	–
Rh/100%ZrO_2–Al_2O_3	54	0.18	0.35	0.46	10.7	3.1	4.1
Rh/ZrO_2	3	–	0.06	–	–	18.3	13.9

as compared with their respective supports (Fig. 1a) suggest that larger tetragonal ZrO_2 crystals are formed as a consequence of Rh impregnation and calcination at 700 °C. These may obstruct the entrance of pores, thus reducing the support surface area [7, 26]. Since the surface area of pure monoclinic ZrO_2 is already very small [7], the impregnation of Rh on this support, followed by calcination at 700 °C for 4 h, barely affects the catalyst surface area.

The XPS measurements indicate that the ZrO_2 dispersion of modified supports and catalysts increases with ZrO_2 loading up to a maximum value for the 75%Zr–Al_2O_3 and Rh/75%Zr–Al_2O_3, but further loading of zirconia into the grafted support results in lower zirconia dispersion, as confirmed by the lower ZrO_2 dispersion observed for the 75%Zr–Al_2O_3 support and Rh/75%Zr–Al_2O_3 catalyst (Table 2; Fig. 2). It is noteworthy that Rh impregnation on modified supports and calcination at 700 °C slightly decrease the ZrO_2 dispersion in the 75%Zr–Al_2O_3 and 100%Zr–Al_2O_3 supports, but significantly increase the ZrO_2 dispersion in the 50%Zr–Al_2O_3 support (Table 2). Nevertheless, the Rh dispersion estimated from CO chemisorption for the grafted-supported catalysts seems to be insensitive to the ZrO_2 dispersion calculated from XPS measurements (Table 2). Fig. 2 also shows that the long-time exposure of catalysts to the DRM reaction conditions does not affect the ZrO_2 dispersion in the catalyst supports, which evidences their high stability.

The grafted-supported Rh catalysts show similar Rh dispersion, and consequently similar mean Rh cluster size, as compared to Rh/0%ZrO_2–Al_2O_3 (d $\sim$ 3.5 nm); the percentage of Rh monolayer dispersion also shows the same trend (Table 2), even though it overestimates the Rh dispersion measured from CO chemisorption and TEM, as explained in the Sect. 2.2. On the other hand, the average Rh cluster size in Rh/ZrO_2 is significantly larger (d = 18.3 nm) than in alumina-containing catalysts. The mean Rh cluster sizes for three selected catalysts were also measured by TEM technique in order to confirm the values estimated by CO chemisorption and XPS, and the results seem to be consistent (Table 2). Since identical calcination

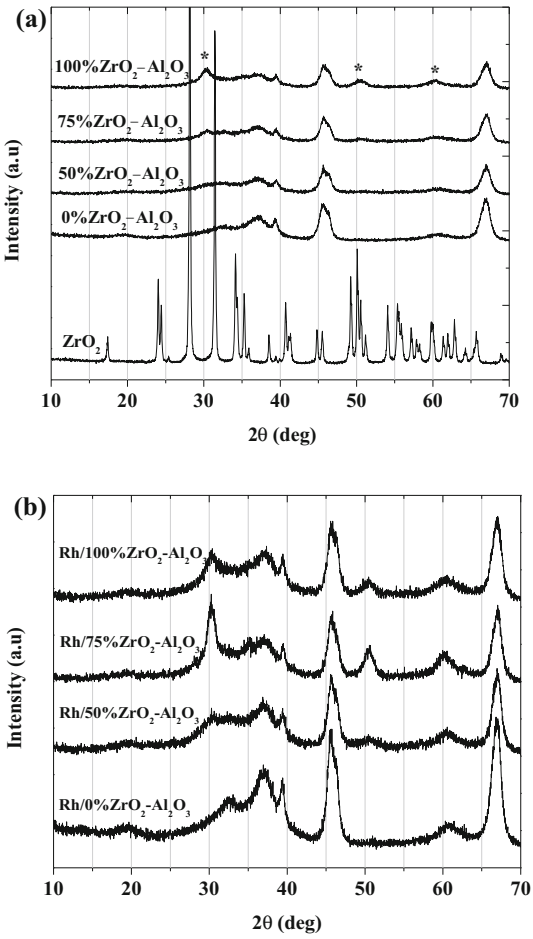

Fig. 1 XRD spectra: **a** supports; **b** catalysts. (*asterisk*) tetragonal ZrO_2 phases

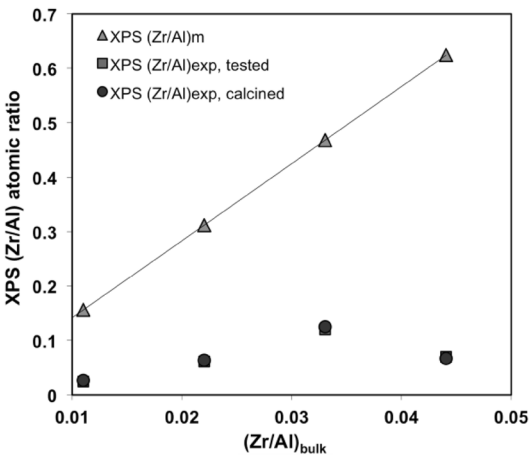

Fig. 2 XPS (Zr/Al) atomic ratio as a function of the nominal (Zr/Al) bulk atomic ratio in ZrO_2–Al_2O_3 supported Rh catalysts. XPS $(Zr/Al)_m$ corresponds to the theoretical monolayer dispersion

procedures were used to prepare all supported Rh catalysts, the huge difference between Rh dispersion on Rh/ZrO_2 and the other catalysts is mainly attributed to the differences in the specific surface area of supports.

The effect of cluster size and Rh-alumina interaction on DRM reaction rate

The CH_4 conversion reported in Table 1 strongly depends on the exposed surface of active phase available in each catalytic test. The catalytic activity in terms of forward reaction rates is calculated according to the procedure detailed in Sect. 2.3, using the Rh dispersion calculated from CO chemisorption, reported in Table 2.

The effect of temperature on the rate constant of methane conversion rate for all supported Rh catalyst is presented in Fig. 3. They confirm the exponential effect of temperature on the rate constant of reaction, and allow calculating the activation energy for the reaction on each catalyst. All catalysts with alumina-containing support show very similar absolute value of rate constant for CH_4 reforming reaction, at each temperature, regardless the degree of zirconia grafting on alumina. Rh/ZrO_2 catalyst is the least active for DRM (it shows the lowest reaction rate value), despite the similar apparent activation energies that are measured for all catalysts tested at similar reaction conditions (Table 1).

The higher activity of catalysts with higher dispersions confirms the well-reported structural sensitivity of CH_4 dry reforming reaction [14, 16, 27]. The larger mean Rh cluster size ($d = 18.3$ nm) in the Rh/ZrO_2 catalyst explains the lower CH_4 conversion rate observed on this catalyst, as compared with the significantly higher rate values obtained on Zr-grafted supported Rh catalysts with an average cluster size of ~ 3 nm. In fact, experimental evidence and theoretical calculations [14, 16, 27] have proved that the activation of the CH_4 molecule is the rate determining step for DRM. This elementary step is favored on smaller clusters, where the percentage of Rh atoms occupying corner and edge positions (low coordinated atoms) is higher than in large clusters. Then, the reaction rate measured on the large rhodium clusters of Rh/ZrO_2 mostly corresponds to the activity of

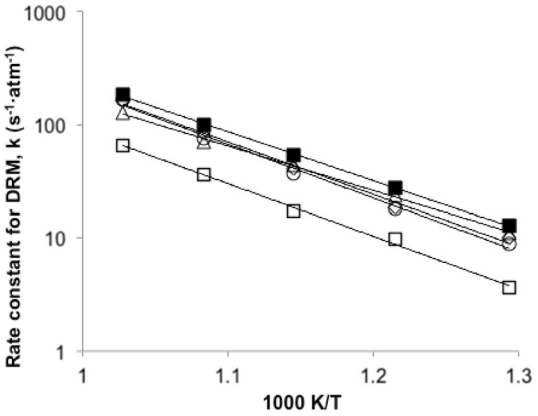

Fig. 3 Arrhenius plots for rate constants of CH_4 reforming reaction. (*circle*) $Rh/0\%ZrO_2$–Al_2O_3; (*diamond*) $Rh/100\%Zr$–Al_2O_3; (*triangle*) $Rh/75\%Zr$–Al_2O_3; (*filled square*) $Rh/50\%Zr$–Al_2O_3; (*open square*) Rh/ZrO_2. Reaction conditions: 10 kPa CH_4/20 kPa CO_2/He balance; 1.2×10^5 mL h^{-1} g_{cat}^{-1}

highly coordinated Rh atoms that slowly activate methane molecules, thus causing a low reaction rate.

TPR experiments were carried out for all catalysts, in order to evaluate the metal-support interaction (Fig. 4) and the extent of reduction of rhodium oxides. The TPR procedure strictly reproduces the pretreatment of catalyst activation performed in each catalytic test, that is, a reduction of the catalyst under pure H_2 and increasing temperature (up to 700 °C), plus a further reduction at 700 °C for 2 h.

Fig. 4 shows only the dynamic heating stage of TPR assays and clearly evidences the stronger Rh-support interaction for the Rh/0%ZrO_2–Al_2O_3 catalyst, as compared with the Rh/ZrO_2 catalyst. Regarding the grafted-supported Rh catalysts, the TPR profiles suggest an intermediate Rh-support interaction that is weaker than in Rh/0%ZrO_2–Al_2O_3, but slightly stronger than in Rh/ZrO_2 catalyst. This suggests that the alumina surface is not fully covered with zirconia via grafting method, which is confirmed by the XPS results (Table 2; Fig. 2). Moreover, the XPS characterization for fresh and tested Rh/0%ZrO_2–Al_2O_3 and Rh/ZrO_2 catalysts is reported elsewhere [7] for similar reaction conditions. It is shown a higher Rh^0 surface content on Rh/ZrO_2 than on Rh/0%ZrO_2–Al_2O_3, which confirms the stronger Rh-support interaction in the latter.

The peak at lower temperatures (100–200 °C) observed for all catalysts is attributed to the isolated RhO_x particles in weak interaction with the support [9, 28]. For the Rh/ZrO_2 catalyst, the well-defined reduction peak at ~90 °C indicates a large extent of Rh reduction, meaning that practically all the supported Rh is reduced at such a low temperature, which is consistent with a weak metal-support interaction for this catalyst. In contrast, the TPR profile for Rh/0%ZrO_2–Al_2O_3 shows a smaller low-temperature peak that appears at a higher temperature (~180 °C), and an additional large H_2 consumption at even higher temperatures (>200 °C). This TPR profile proves the strong Rh-alumina interaction, which is consistent with previous reports [29]. The TPR analyses for grafted-supported Rh catalysts show low-temperature peaks at 120–160 °C, which are mainly attributed to the reduction of rhodium oxides located over the grafted zirconia, and broad peaks

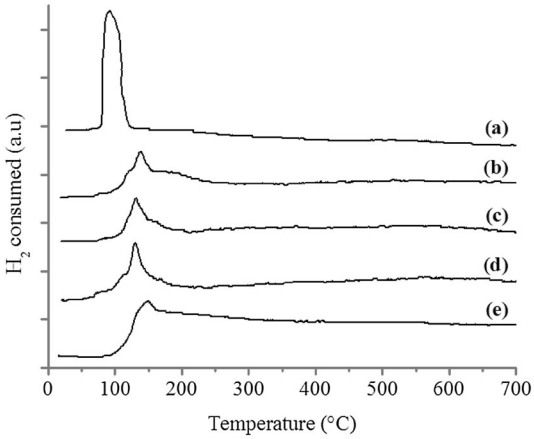

Fig. 4 Temperature program reduction profiles: *a* Rh/ZrO_2; *b* Rh/100%Zr–Al_2O_3; *c* Rh/75%Zr–Al_2O_3; *d* Rh/50%Zr–Al_2O_3; *e* Rh/0%ZrO_2–Al_2O_3

at higher temperatures (>400 °C), representing the reduction of Rh particles in stronger interaction with alumina.

The different nature of the zirconia phases in contact with the supported Rh may play an important role in the Rh-support interaction. As discussed above, XRD characterization demonstrates that tetragonal ZrO_2 phases are formed during the grafting procedure and that the amount and size of these crystals increase with both the loading of zirconia in the support and the high temperature used for the calcination process; therefore, more Rh in contact with tetragonal ZrO_2 is expected to be in the grafted-supported Rh catalysts with higher zirconia content. All supported Rh, however, is in contact only with monoclinic ZrO_2 in the Rh/ZrO_2 catalyst.

It is noteworthy that among the grafted catalysts, the TPR profile of $Rh/50\%Zr–Al_2O_3$ is the most similar to the Rh/ZrO_2 profile, presenting the lowest extent of Rh-support interaction. The catalysts with the larger degree of zirconia grafting ($Rh/75\%Zr–Al_2O_3$ and $Rh/100\%Zr–Al_2O_3$) show the low-temperature reduction peak at higher temperature, which indicates a higher Rh-support interaction, i.e., the following order for Rh-support interaction is assumed (Fig. 4): $Rh/0\%ZrO_2–Al_2O_3 > Rh/100\%Zr–Al_2O_3 > Rh/75\%Zr–Al_2O_3 > Rh/50\%Zr–Al_2O_3 > Rh/ZrO_2$. On the other hand, the dispersion of ZrO_2 on the grafted supports do not follows the same trend (Table 2): $Rh/75\%Zr–Al_2O_3 > Rh/50\%Zr–Al_2O_3 \approx Rh/100\%Zr–Al_2O_3$. It is important to note that this order observed for ZrO_2 dispersion does not necessarily means that the coverage of alumina with zirconia is similar in $Rh/50\%Zr–Al_2O_3$ and $Rh/100\%Zr–Al_2O_3$ catalysts, in fact, is expected that higher ZrO_2 surface is available in the $100\%Zr–Al_2O_3$ support, therefore, more Rh supported over zirconia should be in the $Rh/100\%Zr–Al_2O_3$ than in $Rh/50\%Zr–Al_2O_3$.

These results suggest that both the coverage of alumina with zirconia and the nature of ZrO_2 phase formed in the grafted supports determine the degree of Rh-support interaction in the $ZrO_2–Al_2O_3$-supported Rh catalysts; a higher coverage of alumina with zirconia leads to a catalyst with more Rh in contact with ZrO_2 instead of with Al_2O_3, which decrease the metal-support interaction. However, the results also suggest that the interaction of Rh with the monoclinic phase is weaker than with the tetragonal phase of zirconia, the latter more abundant as the loading of ZrO_2 is increased in the grafted supports, consequently, the Rh-support interaction increases with the content of ZrO_2 in the grafted supported Rh catalyst.

Regardless of the differences in Rh-support interaction between the studied catalysts, it is noteworthy that this interaction has no significant effect on the 'structure sensitivity' feature of DRM reaction on Rh catalysts (explained above). In fact, the reaction rates are similar for catalysts with similar mean Rh cluster size, such as for $Rh/0\%ZrO_2–Al_2O_3$ and $Zr–Al_2O_3$ supported Rh catalysts (Fig. 3), in spite of their differences in Rh-support interaction (Fig. 4). Moreover, the Rh/ZrO_2 catalyst, having the weakest Rh-support interaction presented the lowest activity for DRM, which is attributed to the larger average cluster size of Rh in this catalyst. Therefore, the DRM reaction rate is determined by the coordination degree of Rh atoms on the catalyst surface, which depends on Rh dispersion. However, the Rh-

support interaction has no effect on the DRM reaction rate, unless it influences the Rh dispersion or affects the degree of Rh reducibility in the catalysts.

Conclusions

The grafting of alumina with zirconia has no effect on Rh dispersion since it was observed that grafted-supported Rh catalysts show similar mean Rh cluster size, as compared with the Rh/0%ZrO_2–Al_2O_3, which is attributed to the similar surface area of supports where the Rh precursor was impregnated. In fact, the significantly lower Rh dispersion on Rh/ZrO_2 as compared with the rest of catalysts is exclusively attributed to the differences in the specific surface area of supports.

The strong interaction between Rh-alumina can be decreased and controlled by modifying the alumina with zirconia, prior to Rh precursor impregnation. The coverage of alumina with zirconia and the nature of ZrO_2 phase formed in the grafted supports determine the degree of Rh-support interaction in the ZrO_2–Al_2O_3-supported Rh catalysts; the interaction of Rh with tetragonal ZrO_2 phases seems to be stronger than with the monoclinic phase. However, this interaction does not affect the structural sensitivity of DRM on Rh catalysts. The CH_4 conversion rates result similar for catalysts with similar mean Rh cluster size, regardless their different Rh-support interaction, which confirms that the reaction rate for DRM is determined by the degree of Rh coordination on the catalyst surface, which is inversely proportional to the Rh dispersion.

Acknowledgements The authors thank CONICYT, Fellowship AGCI, FONDECYT (1101005, 1140410, 1130005) and Red Doctoral REDOC, MINEDUC project UCO1202.

References

1. Horiuchi T, Sakuma K, Fukui T, Kubo Y, Osaki T, Mori T (1996) Suppression of carbon deposition in the CO_2-reforming of CH_4 by adding basic metal oxides to a Ni/Al_2O_3 catalyst. Appl Catal A 144(1–2):111–120. doi:10.1016/0926-860X(96)00100-7
2. Centi G, Perathoner S (2009) Opportunities and prospects in the chemical recycling of carbon dioxide to fuels. Catal Today 148(3–4):191–205. doi:10.1016/j.cattod.2009.07.075
3. Karelovic A, Bargibant A, Fernández C, Ruiz P (2012) Effect of the structural and morphological properties of Cu/ZnO catalysts prepared by citrate method on their activity toward methanol synthesis from CO_2 and H_2 under mild reaction conditions. Catal Today 197(1):109–118. doi:10.1016/j.cattod.2012.07.029
4. Li H, Wang J (2004) Study on CO_2 reforming of methane to syngas over Al_2O_3–ZrO_2 supported Ni catalysts prepared via a direct sol–gel process. Chem Eng Sci 59(22–23):4861–4867. doi:10.1016/j.ces.2004.07.076
5. Ferreira-Aparicio P, Fernandez-Garcia M, Guerrero-Ruiz A, Rodrı&guez-Ramos I (2000) Evaluation of the role of the metal-support interfacial centers in the dry reforming of methane on alumina-supported rhodium catalysts. J Catal 190(2):296–308. doi:10.1006/jcat.1999.2752
6. Gadalla AM, Bower B (1988) The role of catalyst support on the activity of nickel for reforming methane with CO_2. Chem Eng Sci 43(11):3049–3062. doi:10.1016/0009-2509(88)80058-7
7. Fernández C, Miranda N, García X, Eloy P, Ruiz P, Gordon A, Jiménez R (2014) Insights into dynamic surface processes occurring in Rh supported on Zr-grafted γ-Al_2O_3 during dry reforming of methane. Appl Catal B 156–157:202–212. doi:10.1016/j.apcatb.2014.03.023

8. Bradford MCJ, Albert Vannice M (1999) The role of metal–support interactions in CO_2 reforming of CH_4. Catal Today 50(1):87–96. doi:10.1016/S0920-5861(98)00465-9
9. Burch R, Loader PK (1996) An investigation of the use of zirconia as a support for rhodium catalysts. Appl Catal A 143(2):317–335. doi:10.1016/0926-860X(96)00089-0
10. Ferreira-Aparicio P, Fernández-García M, Rodríguez-Ramos I, Guerrero-Ruiz A (2000) Support effect over rhodium catalysts during the reforming of methane by carbon dioxide. In: Avelino Corma FVMSM, José Luis GF (eds) Studies in surface science and catalysis, vol 130. Elsevier, Amsterdam, pp 3675–3680. doi:10.1016/S0167-2991(00)80594-7
11. Rostrupnielsen JR, Hansen JHB (1993) CO_2-reforming of methane over transition metals. J Catal 144(1):38–49. doi:10.1006/jcat.1993.1312
12. Therdthianwong S, Siangchin C, Therdthianwong A (2008) Improvement of coke resistance of Ni/Al_2O_3 catalyst in CH_4/CO_2 reforming by ZrO_2 addition. Fuel Process Technol 89(2):160–168. doi:10.1016/j.fuproc.2007.09.003
13. Mateos-Pedrero C, Carrazán SRG, Ruiz P (2006) Surface modifications of γ-Al_2O_3, SiO_2 and SnO_2 supports by titania grafting and their influence in the catalytic combustion of methane. Catal Today 112(1–4):107–111. doi:10.1016/j.cattod.2005.11.057
14. Wei J, Iglesia E (2004) Structural requirements and reaction pathways in methane activation and chemical conversion catalyzed by rhodium. J Catal 225(1):116–127. doi:10.1016/j.jcat.2003.09.030
15. Wei J, Iglesia E (2004) Isotopic and kinetic assessment of the mechanism of reactions of CH_4 with CO_2 or H_2O to form synthesis gas and carbon on nickel catalysts. J Catal 224(2):370–383. doi:10.1016/j.jcat.2004.02.032
16. Ligthart DAJM, van Santen RA, Hensen EJM (2011) Influence of particle size on the activity and stability in steam methane reforming of supported Rh nanoparticles. J Catal 280(2):206–220. doi:10.1016/j.jcat.2011.03.015
17. Kerkhof FPJM, Moulijn JA (1979) Quantitative analysis of XPS intensities for supported catalysts. J Phys Chem 83(12):1612–1619
18. Tanuma S, Powell CJ, Penn DR (1994) Calculations of electron inelastic mean free paths. Surf Interface Anal 21(3):165–176
19. Scofield JH (1976) Hartree-Slater subshell photoionization cross-sections at 1254 and 1487 eV. J Electron Spectrosc Relat Phenomena 8(2):129–137. doi:10.1016/0368-2048(76)80015-1
20. Tougaard S (2002) QUASES-IMFP-TPP2M. QUASES-Tougaard Inc, Denmark
21. Bengaard HS, Nørskov JK, Sehested J, Clausen BS, Nielsen LP, Molenbroek AM, Rostrup-Nielsen JR (2002) Steam reforming and graphite formation on Ni catalysts. J Catal 209(2):365–384. doi:10.1006/jcat.2002.3579
22. Djéga-Mariadassou G (1984) Kinetics of heterogeneous catalytic reactions. Princeton University Press, Princeton, p 1984
23. Fogler HS (2001) Elementos de ingenieria de las reacciones quimicas, 3rd edn. Prentice-Hall, Upper Saddle Rive
24. Levine IN (1996) Físico química, vol 2, 4th edn. McGraw Hill, New York
25. Lide DR (ed) (2005) CRC handbook of chemistry and physics. CRC Press, Boca Raton
26. Damyanova S, Grange P, Delmon B (1997) Surface characterization of zirconia-coated alumina and silica carriers. J Catal 168(2):421–430. doi:10.1006/jcat.1997.1671
27. Vannice MA (2005) Kinetics of catalytic reactions. Springer, New York
28. Burch R, Loader PK, Cruise NA (1996) An investigation of the deactivation of Rh/alumina catalysts under strong oxidising conditions. Appl Catal A 147(2):375–394. doi:10.1016/S0926-860X(96)00212-8
29. Ojeda M, Nabar R, Nilekar AU, Ishikawa A, Mavrikakis M, Iglesia E (2010) CO activation pathways and the mechanism of Fischer–Tropsch synthesis. J Catal 272(2):287–297. doi:10.1016/j.jcat.2010.04.012